Nondestructive damage detection of concrete with alkali-silica reactions using coda wave and anomaly detection

Taeyong Shin, Hongbin Sun, Jinying Zhu, and Ying Zhang

***Abstract*— An anomaly detection model for early damage detection for concrete structures undergoing alkali-silica reaction (ASR) is presented. It is difficult to detect ASR initiation and early damage without a reference expansion measurement. Coda waves, or the multiply scattered portion of ultrasonic waves, have been found to be indicative of small changes in complex material such as concrete. The relationship between concrete damage and relative velocity change and decorrelation of coda waves has been studied, but a generalized model which detects when damage occurs in a concrete structure is still lacking. The presented method uses features extracted from coda waves to detect early damage in concrete structures. The model uses unsupervised learning and only requires data from undamaged structures for training. During the training process, the reconstruction error of the training data is minimized. When the data collected from damaged concrete structures is used as an input of the model, it returns high reconstruction errors that indicate the occurrence of damage in the structures. The performance of the model is validated using experimental studies and has been shown to generalize across two different ASR specimens.**

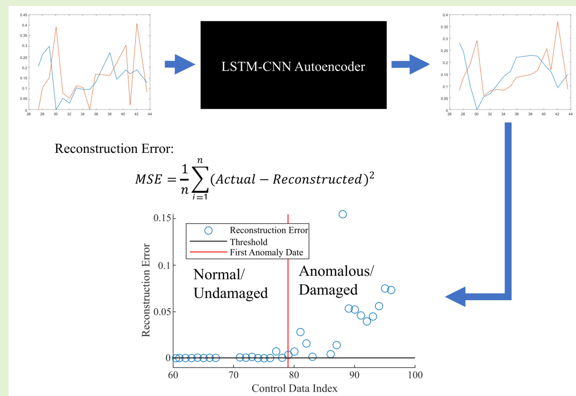

***Index Terms*— anomaly detection, ultrasonic coda wave, concrete, alkali-silica reaction**

I. Introduction

ALKALI-silica reaction (ASR) is a chemical reaction that occurs between the reactive silica present in aggregates and the alkali components present in the cement of concrete structures. The reaction produces a gel that causes tensile stress within a concrete structure, leading to crack initiation, propagation, and eventual failure [1]. ASR is a major issue for many existing concrete structures including bridges, dams, and power plants. However, because ASR is a slow process, it may take many years before surface cracks are observable. At this point, it may be difficult to inhibit the progress of ASR damage [2]. Therefore, a method to detect the small changes in the material before the damage is too extensive is required.

Many researchers have investigated using coda waves for detecting small changes in concrete structures. The word coda, which has been adopted from the seismological community, refers to tail of a seismogram after an earthquake [3]. The tail consists of late arrivals affected by interference of various wave trajectories. Similarly, coda can be observed in ultrasonic signals, which have passed through a solid structure and have late arrivals caused by scattering within the material. The scattered waves spend a longer time in the material than direct waves and have been found to be more sensitive to small changes in the material [4].

Numerous methods have been investigated by researchers [4], [5], [7]–[13] to monitor damage in concrete using coda wave based on the velocity variation and decorrelation of coda waves. Zhang et al. [7] have found that the velocity variation of coda waves is inversely proportional to the tensile stress, demonstrating the ability to estimate tensile stress changes in concrete. Larose and Hall [12] have suggested that weak stretching and strong distortion of coda waves may indicate a change of structure rather than a global velocity change. These trends of coda wave change have been used to characterize

This paragraph of the first footnote will contain the date on which you submitted your paper for review. It will also contain support information, including sponsor and financial support acknowledgment. For example, "This research is supported in part by the U.S. Department of Energy - Nuclear Energy University Program (NEUP) under the contract DE-NE0008544."

T. Shin is with the School of Electrical & Computer Engineering, Georgia Institute of Technology, Atlanta, GA 30332, U.S.A (e-mail: taeyongshin@gatech.edu).

H. Sun was with the Department of Civil and Environmental Engineering, University of Nebraska-Lincoln, Omaha, NE 68182, USA. He is now with the Oak Ridge National Laboratory, Oak Ridge, TN 37830, USA (e-mail: sunh1@ornl.gov).

J. Zhu is with the Department of Civil and Environmental Engineering, University of Nebraska-Lincoln, Omaha, NE 68182, USA (e-mail: jyzhu@unl.edu).

Y. Zhang is with the School of Electrical & Computer Engineering, Georgia Institute of Technology, Atlanta, GA 30332, U.S.A (e-mail: yzhang@gatech.edu).

changes in concrete.

However, there is still a need for a generalized method that can determine when damage occurs in real time based on coda wave measurements provided by a structural health monitoring system. Some researchers have attempted to develop methods to monitor damage. Most methods have focused on demonstrating that measured coda wave features are related damage indicative measurements such as applied stress or expansion. For example, in [5]–[7] the authors showed that there is a correlation between coda wave features, such as velocity variation and the slope of velocity variation, and damage in concrete specimens. These methods have showed that coda wave features will change as more load is applied to concrete specimens. A greater amount of load applied resulted in a greater amount of change in the coda wave features. However, because acousto-elasticity depends on the make-up of the material, the amount of change caused by a specific amount of applied load varied from sample to sample [4]. For example, a feature value change of 5% may be indicative of damage for one specimen but not for another. Furthermore, in [11], Zhang et. al discuss a method of monitoring stress and damage development on a 15-ton concrete beam undergoing a four-point bending test. By using kernels of diffuse waves to describe the spatial sensitivity of ultrasound to local elastic and structural changes, an imaging procedure to locate and map changes occurring in a 15-ton concrete beam has been proposed. This method however, also requires parameters that are obtained using onsite measurements to develop their model. The study proposed in this paper focuses on developing a more generalized damage detection model that requires only measurements from some concrete specimens in undamaged states, and can be applied to other specimens to predict the initiation of damage using the coda wave measurements collected in real time.

Anomaly detection is a potential approach for detecting the occurrence of damage in various applications. Anomaly detection refers to the problem of finding patterns in data that do not conform to the expected behavior [14]. Correctly identifying areas which deviate from the norm is an important problem in many applications. For example, Jiang and coauthors suggested using reconstruction-error based anomaly detection for defect detection of wind turbines [15]. Alex et. al. proposed an anomaly detection method to detect brain lesions using magnetic resonance images [16]. In the structural health monitoring field, Chow et. al. proposed using a convolutional autoencoder to detect surface cracks in concrete structures using image data [17].

The studies mentioned above use a reconstruction-error-based anomaly detection. The advantages of such a method is that a model can be trained without the need for labeled data and that it has been shown to generalize across different specimens. For many applications, normal data is abundant and can be readily collected. However, anomalous data can be scarce, hard to collect, and hard to identify. A reconstruction-error-based anomaly detection method is not hindered by this issue as it only requires normal data for training of the model. Any sufficient deviation from the normal training data is considered to be an anomaly, suggesting a change in the material. A major disadvantage of reconstruction-error-based anomaly detection methods is that a large number of training samples are required. However, this should not be an issue as data from undamaged concrete structures is readily collectable.

Inspired by previous work, a reconstruction-error-based anomaly detection method is proposed for detecting ASR damage initiation in concrete. The method is based on an autoencoder that utilizes convolutional and recurrent layers, hereon referred to as the Long Short-Term Memory Convolutional neural network (LSTM-CNN) autoencoder. The LSTM-CNN autoencoder attempts to extract the representational and local features of relative velocity variation and decorrelation of coda waves. Then, by using a reconstruction-error based anomaly detection method, a model is developed to identify crack initiation in concrete. Experimental studies are conducted for model development and validation of the model's effectiveness.

II. Methodology

A reconstruction-error based anomaly detection method is proposed to detect the initiation of ASR damages in concrete using coda waves. Instead of using the raw coda waves as inputs for the anomaly detection model, small input sequences are created using the damage indicative traits, velocity variation, and decorrelation, since certain behaviors of the velocity variation and decorrelation have been shown to be representative of changes in complex material. An autoencoder is used to extract the features of the velocity variation and decorrelation sequences. Then, using these extracted features, the autoencoder is trained to reconstruct the input sequence. The reconstructed sequences are compared to the original input sequences using mean-squared error to obtain a measure of reconstruction error. The reconstruction error is then used to determine whether or not an input sequence is anomalous. Fig. 1 illustrates the main steps of the reconstruction-error-based anomaly detection method.

A. Damage Indicative Features

1) Coda Wave Interferometry: Coda waves are an ensemble average of all the waves coming to the ultrasonic sensor from any direction. The early portions of the signal represent the waves from the shortest path between the transducer and the receiver. The later portions have traveled further through the material and have been subject to multiple scatterers [18]. Because the later portions propagate further and are more affected by scatterers in the material, they have been shown to be more sensitive to small changes in the material. This is illustrated by Fig. 2. Although the early portions of the signals, shown in the top inset of Fig. 2, are almost identical for both the reference signal, collected before changes occur within the material, and the perturbed signal. The later portions (coda waves), shown in the bottom inset of Fig. 2, show a significant difference (amplitude and phase), indicating changes in the material.

ASR-induced microcracks may not be readily detected by conventional ultrasonic methods using coherent waves at the early stage, but these small changes could be captured by the coda wave which is the result of wave multiple scattering on

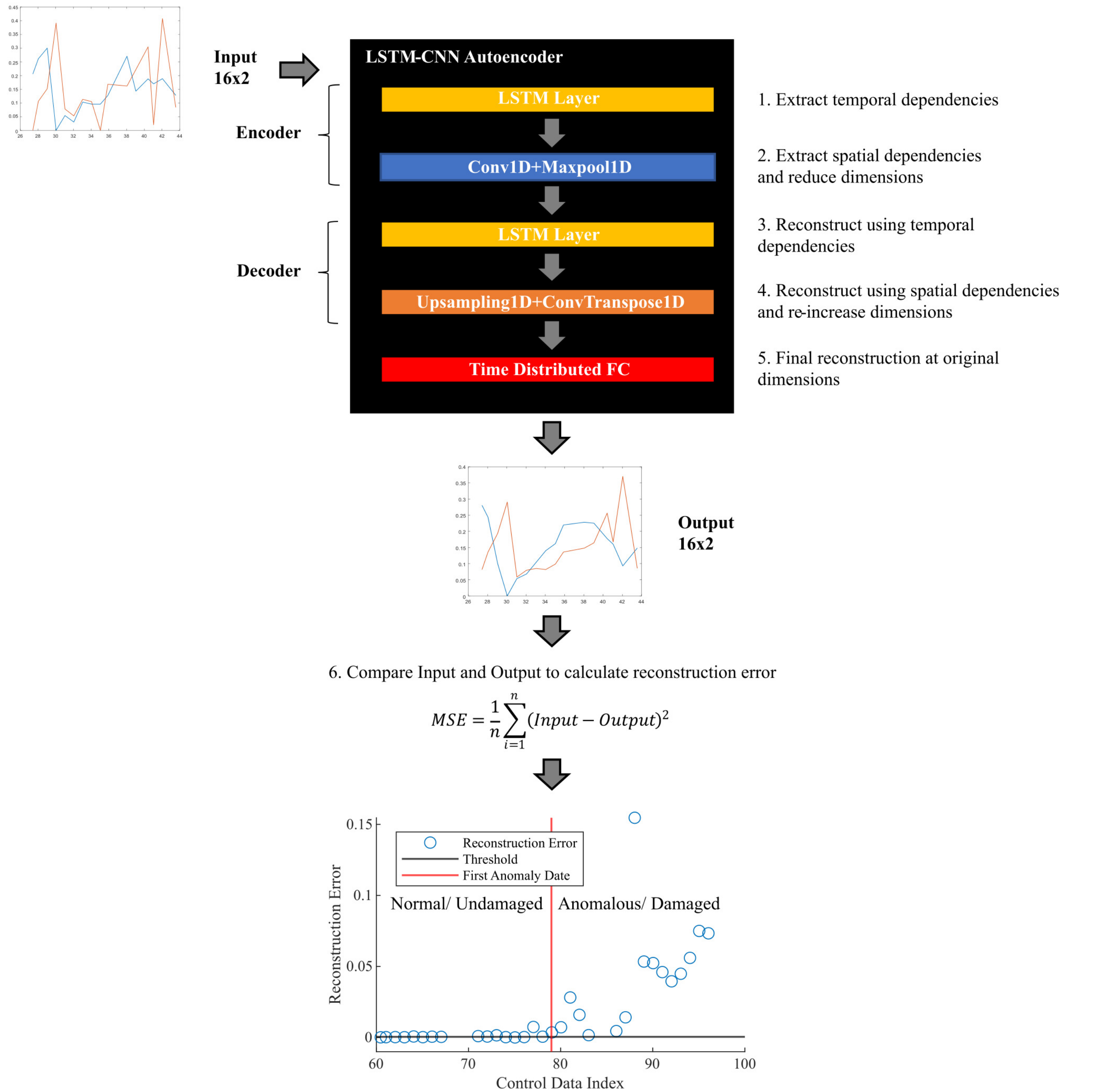

Fig. 1. Flowchart of steps using the LSTM-CNN Autoencoder for anomaly detection

these microcracks. The coda wave could amplify these small changes in concrete. Therefore, coda wave could be used for monitoring the ASR development in concrete.

The technique of analyzing the small changes in the coda wave is called coda wave interferometry (CWI). Snieder et al. proposed a method to determine this velocity change in solid materials by correlating two similar signals collected on a structure at different times [18]. The signal collected first is used as the reference signal, $s_0(t)$, as it is collected before a change, or a perturbation occurs in the material. The second signal is referred to as the perturbed signal, $s_k(t)$. Then, Lobkis and Weaver proposed a more stable method called the stretching method [20]. For this method, a longer time window, T, is used to compare the reference signal and the perturbed signal than Snieder et al's original method. It is assumed that the relative velocity change is constant within the time window of interest. A stretch factor, ϵ, is used to stretch the perturbed signal to correlate with the reference signal. The optimal stretch factor, ϵ_o, which maximizes the correlation coefficient between the reference signal and the stretched perturbed signal, shown in Fig. 3, is the relative velocity variation. The correlation coefficient between the two

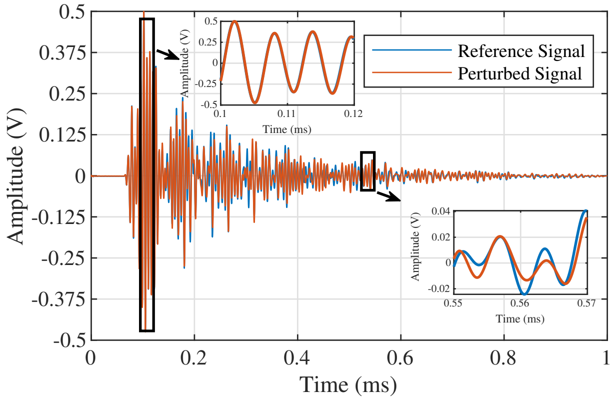

Fig. 2. Reference and perturbed signals for a concrete block. The top inset shows early portion of signals from 0.1ms to 0.12ms, and bottom inset shows later portion of signals from 0.55ms to 0.57ms.

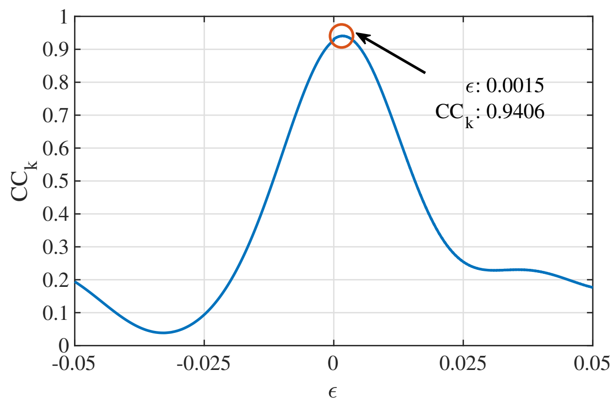

Fig. 3. CC_k vs Epsilon of coda waves shown in Fig. 1.

signals is calculated using (1).

$$CC_k = \frac{\int_{-T/2}^{T/2} s_k(t(1+\epsilon))s_0(t)\,dt}{\sqrt{\int_{-T/2}^{T/2} s_k^2(t(1+\epsilon))\,dt \int_{-T/2}^{T/2} s_0^2(t)\,dt}} \quad (1)$$

This velocity variation feature has been shown to increase under compressive stress and decrease under tensile stress, exhibiting its ability to detect damage in concrete structures [5]. A test conducted with noise introduced into the signal have also shown that velocity variation is robust to noise and can be retrieved as long as a certain portion of the sources is stable [21].

2) Coda Wave Decorrelation: Changes in solid materials, such as concrete, have been found to not only cause amplitude differences and phase shifts, but also cause distortion of signals. Velocity variation best captures the phase changes between the reference signal and perturbed signal, while decorrelation has been found to be a better representation of distortions induced by cracks. Coda wave decorrelation (CWD) calculates the residual distortion of the signal after phase changes have been accounted for as shown in (2) [10].

$$Kd = 1 - CC_k(\epsilon_0) \quad (2)$$

In the example shown in Fig. 3, the maximum correlation coefficient occurs at the stretching factor 0.0015 with the decorrelation 1-0.9406=0.0594. Because the decorrelation is calculated after accounting for velocity variation, it is a measure of changes in the coda wave caused by factors other than temporal stretching, such as distortion by localized defects.

3) Reference Updating Algorithm for Coda Wave Feature Extraction: If too much distortion is present, CWI fails as the velocity variation calculations are no longer meaningful. To combat this issue, researchers have proposed a variety of methods to update the reference signal when necessary. In [22], Zotz-Wilson et. al proposed using a rolling reference, in which a new reference is chosen after a predetermined number of measurements. Niederleithinger et al. proposed two methods of updating the reference. First, they proposed a stepwise method, in which the reference signal is updated after each measurement. Second, they proposed an automated, data-driven procedure for selecting a new reference signal for coda wave interferometry [8]. The authors propose that when the correlation coefficient found using CWI exceeds a predetermined threshold, the reference should be switched to the current signal. The proposed automated method has been shown to decrease the number of reference changes compared to the rolling reference method or the stepwise method, and have shown to reduce rounding errors associated with frequent reference changes. In this paper, that threshold is chosen as 0.9, similar to the value used in [28], and the reference is updated when correlation coefficients fall below this value.

B. Reconstruction-Error Based Anomaly Detection

For early damage detection in concrete, an autoencoder was trained to reconstruct short sequences of velocity variation and decorrelation collected on undamaged control specimens. More information about the control specimen is provided in section III. The autoencoder consists of an encoder-decoder network. The encoder portion of an autoencoder extracts features from the input by reducing the input data to a lower dimensional representation. The decoder portion then uses this lower dimensional representation to reconstruct the original input. This encoder-decoder network is trained to minimize the error of this reconstruction. The reconstruction error of each feature is found using the mean squared error (MSE) equation given by (3), where y_i is the input data point and $\tilde{y}_i$ is the reconstructed data point.

$$MSE = \frac{1}{n}\sum_{i=1}^{n}(y_i - \tilde{y}_i)^2 \quad (3)$$

The reconstruction errors of the two features are then averaged to gain an overall reconstruction error of the data.

If such a network is trained only on normal data, or in our study data collected from undamaged concrete structures, the model will be able to reconstruct data from undamaged concrete structures with very small reconstruction error. However, if the model is used to reconstruct input data representative of a damaged structure, the model will return a high reconstruction error [14]. Therefore, the reconstruction error of the model can be used as a damage indicator.

To utilize the time-dependent patterns of the coda wave features, the coda wave features were organized into sequences. The sequences were created using a fixed-width sliding window of length sixteen and a sliding step size of one. To further preprocess our data, each feature was normalized using a Min-Max scaling method to normalize the features of the training data from zero to one. The preprocessed sequences were then used as inputs for our LSTM-CNN autoencoder.

Furthermore, to determine if an input sequence is an anomaly, or damaged, a reconstruction error threshold must be chosen to make a binary classification. If the reconstruction error falls below the threshold, it is classified as normal, or undamaged, and if the reconstruction error falls above the threshold it is classified as anomalous, or damaged. This threshold is chosen during the training. During training, the reconstruction error of every sequence in the training set is collected. The threshold was then chosen using the interquartile range (IQR). IQR is often used to measure the statistical dispersion and data variability of data by dividing the data into quartiles based on their magnitude. Q1 is defined as the median of the bottom half of the data set based on magnitudes, Q2 is defined as the median of the entire data set, Q3 is defined as the median of the top half of the data set, and Q4 is defined as the maximum value of the entire data set. The interquartile range is defined as the difference between the Q3 and Q1, or IQR=Q3-Q1. A standard method of identifying anomalies in data uses (Q3+1.5×IQR) to determine the threshold [19].

Lastly, for our implementation, a specific date was considered anomalous only if every sequence including data from that date returned a reconstruction error greater than the threshold. Because the length of an input sequence of our model is sixteen, a date is considered an anomalous date only if sixteen consecutive sequences including the corresponding data return reconstruction errors exceeding the threshold. This criterion was enforced for the anomaly detection method because we are not worried about point outliers, but are more concerned with collective outliers. A point outlier is a single point which extremely deviates from well defined norms. A collective outlier, on the other hand, group of data points that fall extremely far from well defined norms of a data set [23]. Point outliers can occur due to reasons that do not necessarily indicate damage in concrete. Sensor malfunctions and environmental changes, for example, can cause point outliers in the measured data when there is no damage to the concrete specimen, but data measured from a damaged concrete specimen will exhibit a shift in the data through consecutive measurements. Using this criterion, the training data returns no anomalous dates, which will be discussed in section IV. Although about 10% of the samples exist above the threshold, there are no instances for which there are more than sixteen consecutive samples exhibiting reconstruction errors above the chosen threshold.

C. Autoencoder Architecture

For the proposed autoencoder, a recurrent layer and a 1-d convolutional layer are used due to the nature of our data. The two main advantages of using a convolutional layer are their computational efficiency as well as their ability to extract features from raw data, while recurrent layers have the advantage of being able to capture changes over time. To determine the number of hidden layers, the number of nodes, and the number of epochs that the model is trained, 3-fold cross validation was used. Only the control data was used for training and validation. After determining the aforementioned hyperparameters, the model was retrained on the entire control data set for optimal model performance [24].

TABLE I
LSTM-CNN AUTOENCODER HYPERPARAMETERS

Layer #	Layer Type	# of Units	Output Shape
1	Input	N/A	16 × 2
2	LSTM	32	16 × 32
3	Conv1D & Maxpool1D	32	8 × 32
4	LSTM	16	8 × 16
5	Conv1D & Maxpool1D	32	4 × 16
6	LSTM	4	4 × 4
7	Conv1D	4	4 × 4
8	LSTM	4	4 × 4
9	Upsampling1D & Conv1DTranspose	16	8 × 16
10	LSTM	16	8 × 16
11	Upsampling1D & Conv1DTranspose	32	16 × 32
12	LSTM	32	16 × 32
13	Time Distributed Fully Connected	2	16 × 2

1) Convolutional Layers: Convolutional layers perform a convolution operation using kernels, or a small matrix of weights, of a predefined size. The kernel slides over the input data computing the dot product, or convolving, with the part of the input it is currently on. For example, given a kernel, w, of length p and an input matrix, x, the resulting matrix, h, of the convolution operation for a 1-dimensional matrix is given by (4).

$$h[i] = \sum_{k=0}^{p-1} x[i+k]w[k] \tag{4}$$

This operation produces an activation map of that kernel. The activation maps act as filters which activate when a specific feature is detected at some spatial position in the input. The filters are therefore able to detect patterns occurring in groups equal to the size of the kernel. By using a different kernel size for each convolutional layer, both general features, learned by using a larger kernel size, and more local features, learned by using a smaller kernel size, can be extracted from the raw data [25]. Because our data is sequential, a 1-dimensional convolutional layer was used, and zero-padding was used to maintain the shape of the input data.

2) Recurrent Layers: Recurrent layers make use of information from the input x_t at time t as well as information from the previous hidden state h_{t-1}, allowing the network to hold information about previous inputs in the sequence. This makes recurrent layers ideal for sequential data. The hidden state, h_t, of the recurrent neural network is found using (5) where W_x and W_h are matrices learned during the training process and f is the activation function.

$$h_t = f(W_x x_t + W_h h_{t-1}) \tag{5}$$

However, the vanilla RNN has been found to face the vanishing gradient problem when dealing with long-term dependencies. Therefore, for this model long-term short-memory (LSTM) layers were used as the recurrent layers. The LSTM layer makes use of gates, the forget gate, the input gate, and the output gate, to regulate the cell state to allow learning of long-term dependencies. The forward pass of the LSTM layer is given by:

$$f_t = \sigma(W_x^{(f)} x_t + W_h^{(f)} h_{t-1} + b^{(f)}) \tag{6}$$

$$i_t = \sigma(W_x^{(i)} x_t + W_h^{(i)} h_{t-1} + b^{(i)}) \tag{7}$$

$$o_t = \sigma(W_x^{(o)} x_t + W_h^{(o)} h_{t-1} + b^{(o)}) \tag{8}$$

$$c_t = f_t \odot c_{t-1} + i_t \odot tanh(W_x^{(c)} x_t + W_h^{(c)} h_{t-1} + b^{(c)}) \tag{9}$$

$$h_t = o_t \odot tanh(c_t) \tag{10}$$

Here, b refers to the bias value, W, refers to the weights, and the superscripts f, i, and o describe which gate the bias and weights refer to, the forget gate, input gate, and output gate respectively. Furthermore f_t, i_t, and o_t are the activation vectors of the forget gate, input gate, and output gate respectively, and c_t is the cell state.

3) Model Implementation: For the proposed model, a time-step of sixteen was used to create short sequences of velocity variation and decorrelation which represent the current status of a concrete specimen, as described in II-B. Then, these short sequences were used as inputs for the autoencoder anomaly detection model. After experimenting with different architectures, a LSTM-CNN model has been found to perform better than a CNN-LSTM model. Zhang et al. have also found this to be true in their model for text classification. They have found that a LSTM-CNN model causes lower feature loss than CNN-LSTM models [26].

For the encoder part of the encoder-decoder architecture, LSTM layers were first used to generate a new encoded sequence containing temporal features of the original input sequence. Next, convolutional layers were used to extract time-invariant, spatial features from the output of the LSTM layer before it. Then, a maxpooling layer was used to reduce redundant features found by the preceding layers and to reduce the dimensionality. The process was then repeated on the features extracted by the convolutional layer and maxpooling layer. A LSTM layer was used to generate an encoded sequence containing temporal features from the features extracted by its preceding layers and a convolutional and maxpooling layer followed that LSTM layer. The decoder part of the encoder-decoder architecture was the inverse of the encoder structure, where a transpose convolutional layer was used as the inverse of the convolutional layer and an upsampling layer was used as an inverse of the maxpooling layer. The model architecture is shown below in Fig. 4. The hyperparameters of the autoencoder model is shown in Table I.

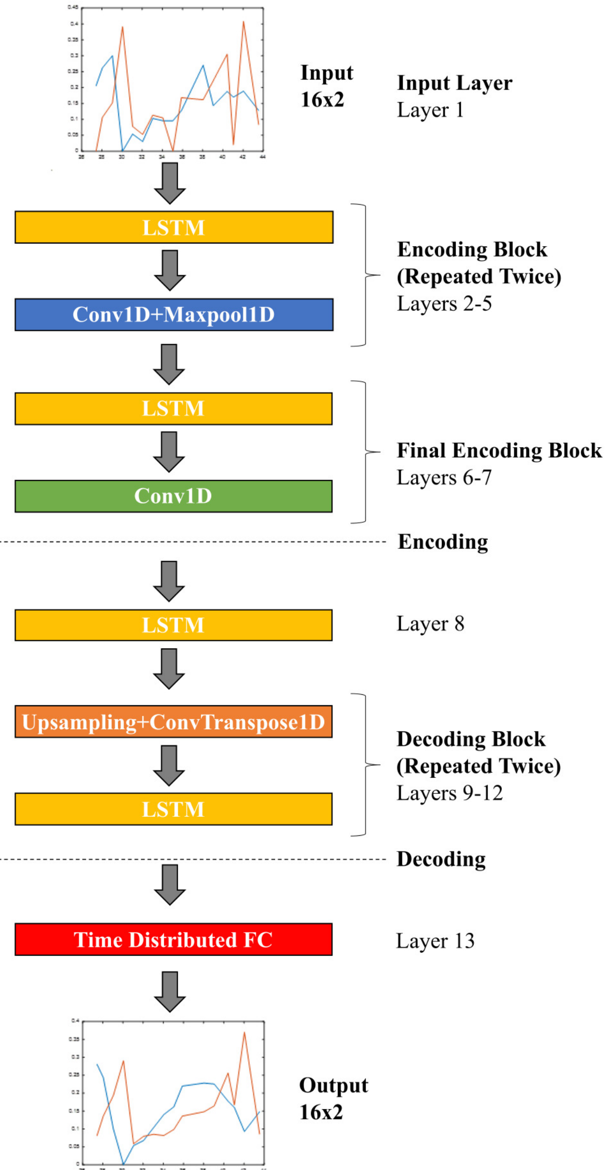

Fig. 4. Anomaly detection model architecture where FC is a fully connected layer.

III. Experimental Setup and Data Collection

Experimental data collected on control and ASR concrete specimens were used to develop and test the performance of the autoencoder anomaly detection model. The data include expansion measurements and ultrasonic signals. The measured expansions were used to indicate damage initiation in each reactive specimen. Ultrasonic signals were used to calculate velocity variation and decorrelation using CWI and CWD respectively before being restructured as inputs for the anomaly detection model.

A. Concrete Specimens

Four concrete samples with dimensions 0.3m × 0.3m × 1.12m were cast. Two control specimens contained non-reactive coarse and fine aggregates while two reactive specimens contained reactive coarse aggregates and sodium hydroxide (NaOH). NaOH solution was added to boost the alkali content to promote rapid ASR in the two reactive samples. Furthermore, one of the control specimens and one of the reactive specimens were reinforced with No. 6 (diameter: 19 mm) headed reinforcement steel to constrain the expansion in the longitudinal and vertical directions. These specimens are herein referred to as the confined specimens. The images of the exterior of the specimens and configuration of reinforcement bar inside the confined specimens are shown in Fig. 5. More details about the concrete samples can be found in reference [27].

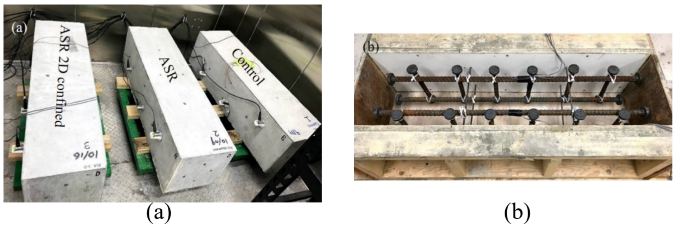

Fig. 5. (a) Concrete specimens placed in the chamber (b) configuration of the reinforcement bar inside the confined specimens [27], [28].

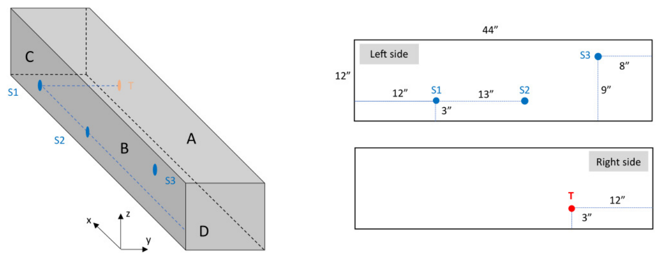

Fig. 6. Sensor positions on concrete specimens [28].

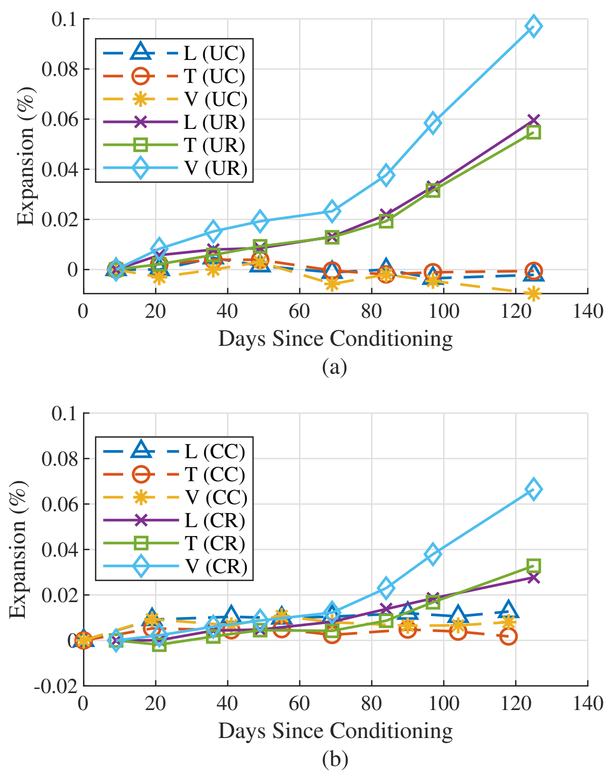

Fig. 7. Expansion of (a) unconfined control and reactive specimens (b) confined control and reactive specimens (L: longitudinal direction (x); T: transverse direction(y); v: vertical direction (z); UC: unconfined control specimen; UR: unconfined reactive specimen; CC: confined control specimen; and CR: confined reactive specimen).

The concrete specimens were moist cured for a minimum of 28-days. Expansion measurements indicate that the ASR reactivity was very low during the curing time. After curing was completed, the samples were moved to an environmental chamber and exposed to a high temperature (38°C) and high humidity (95%) condition. Demountable mechanical strain gauge (DEMEC) targets were installed on each surface of the samples in two directions. The expansions were measured using DEMEC strain gauges (Mayes Instruments Limited, UK) every two weeks when the chamber was shut down, and the internal and surface temperatures of all samples were dropped to 23°C [29].

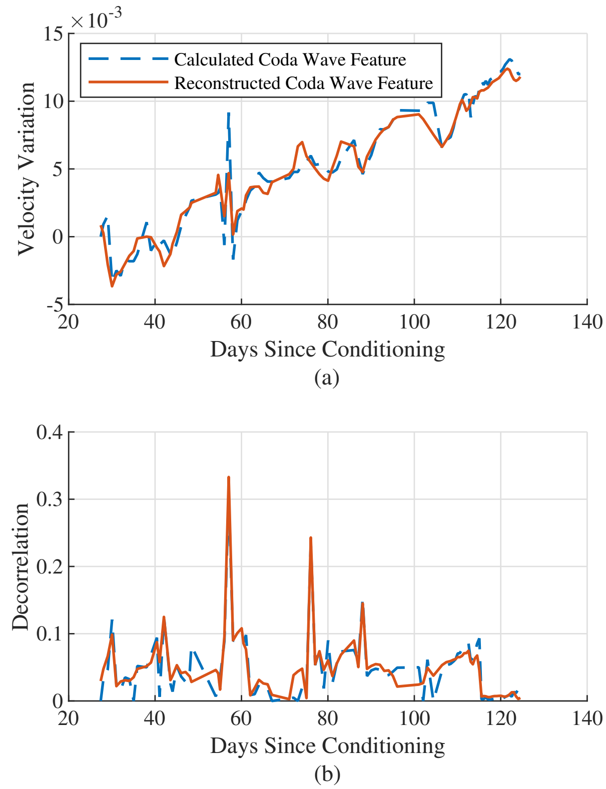

Fig. 8. Comparison of (a) velocity variation and (b) decorrelation between reconstructed values and calculated values using S1 data collected from unconfined control specimen using proposed method.

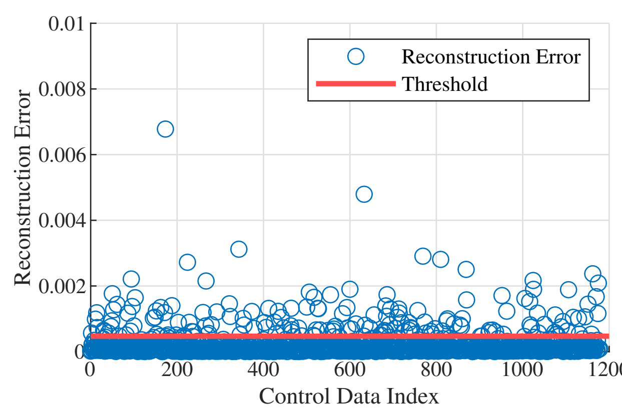

Fig. 9. Reconstruction error of training data

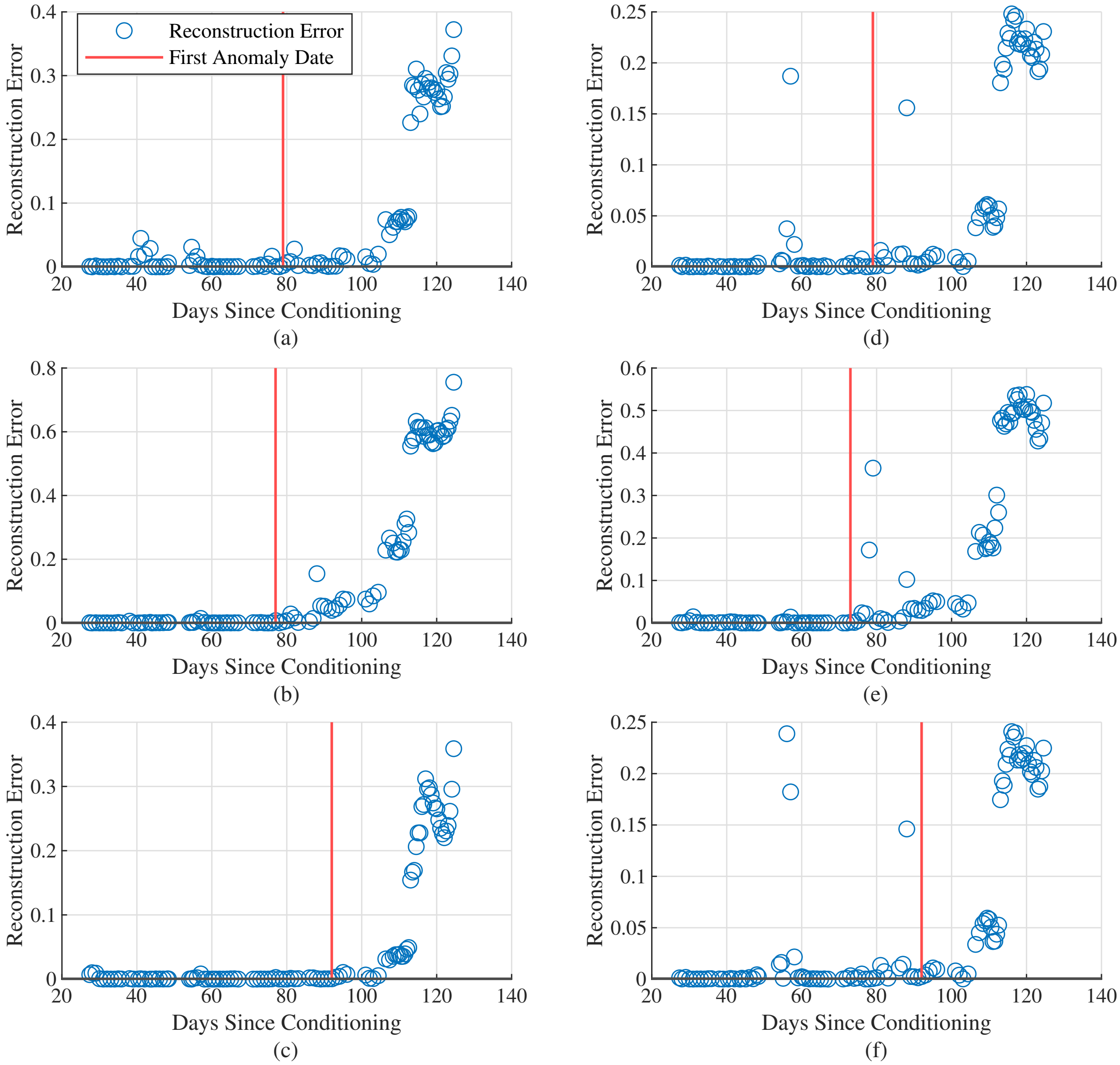

Fig. 10. Reconstruction errors of (a-c) unconfined reactive specimen and (d-f) of the confined reactive specimen (Top: S1, Middle: S2, Bottom: S3 respectively).

TABLE II
FIRST ANOMALY DETECTION DATES FROM ALL SENSORS ON ASR SPECIMENS USING LSTM-CNN AUTOENCODER

Reactive Specimen Type	Sensor Location	Anomaly Detection Date (days since conditioning)
Unconfined	S1	79
	S2	77
	S3	92
Confined	S1	79
	S2	73
	S3	79

TABLE III
FIRST ANOMALY DETECTION DATES FROM ALL SENSORS ON ASR SPECIMENS USING ONE-CLASS SVM

Reactive Specimen Type	Sensor Location	Anomaly Detection Date (days since conditioning)
Unconfined	S1	76
	S2	62
	S3	75
Confined	S1	71
	S2	60
	S3	71

B. Sensor Setup

Three ultrasonic sensors (R6I-AST and R15I-AST, Physical Acoustic, NJ, USA) were installed on each of the four concrete specimens to act as ultrasonic receivers, as shown in Fig. 6. A piezoceramic (PZT) disk (T) was installed on the right-side surface to act as the ultrasonic transmitter and was positioned opposite to sensor S1. During different phases of the experiment, specific sensors were activated to receive ultrasonic

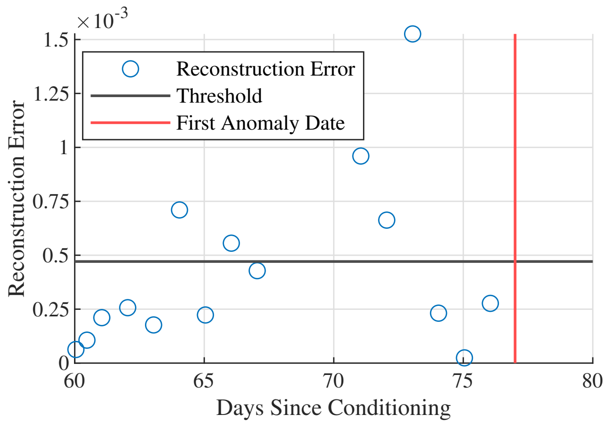

Fig. 11. Reconstruction errors of S2 of the unconfined reactive specimen before the first anomaly date.

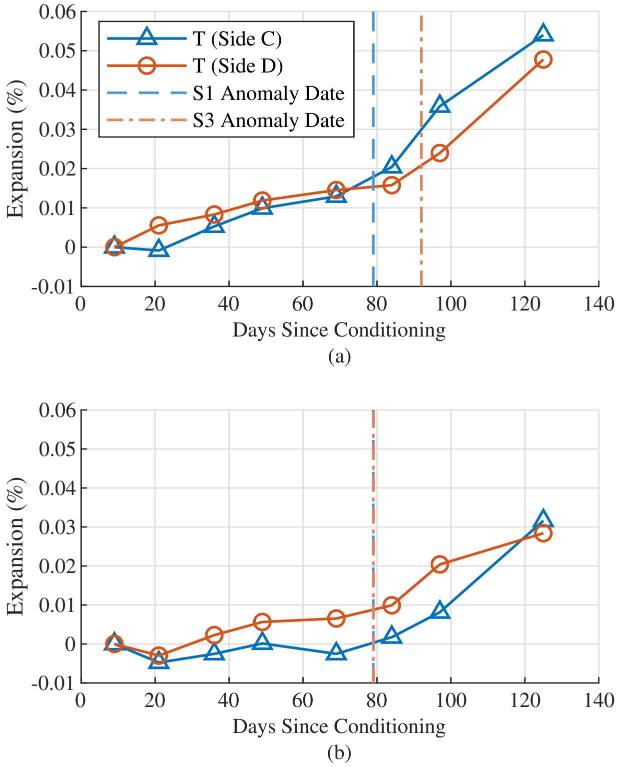

Fig. 12. Axial expansion measurements of (a) transverse axis of sides C and D of the unconfined reactive specimen (b) transverse axis of sides C and D of the confined reactive specimen (T: Transverse Axis).

signals from the transmitter. At 1:05 a.m. and 1:05 p.m. every day, an ultrasonic pulser/receiver (Olympus 5077PR) emitted square wave pulses to drive the transmitter around a central frequency of 100 kHz. The transmitted signals were then received by the activated sensors. The received signals were digitized by an oscilloscope (PICO4262) with a sampling rate of 10 MHz [28]. In this paper, the data collected at 1:05 a.m. of a day is labeled as the measurement on that day, and the data collected at 1:05 p.m. is labeled as the measurement half day past that day. For example, measurements taken at 1:05

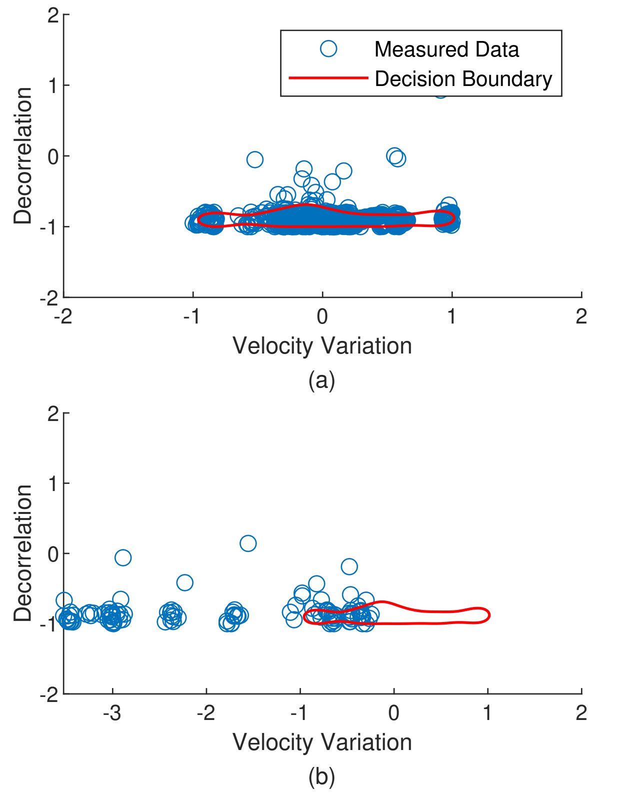

Fig. 13. Decision boundary of one-class SVM for (a) training data (b) testing data of S2 data from unconfined reactive specimen

TABLE IV
FIRST ANOMALY DETECTION DATES FROM ALL SENSORS ON ASR SPECIMENS USING STANDARD AUTOENCODER

Reactive Specimen Type	Sensor Location	Anomaly Detection Date (days since conditioning)
Unconfined	S1	77
	S2	62
	S3	75
Confined	S1	71
	S2	63
	S3	71

a.m. and 1:05 p.m. on day 20 are labeled as measurements on day 20 and day 20.5 respectively. Details of the ultrasonic monitoring system are described by Sun [28].

C. Concrete Expansion

Fig. 7 shows the expansion of each specimen that were taken every two weeks. Both control specimens showed very little expansion throughout the duration of the experiment. The reactive specimens showed very little expansions before day 69, but exhibited a sudden increase in expansion after day 69, as shown by the change in slope. The day at which the slope of the expansion began to increase significantly, between days 69 and 84, was used to represent the estimated date of damage initiation [28]. For both reactive specimens, the expansion measurements show a significant increase between days 69 and 84. The trend is most noticeable in the vertical expansion

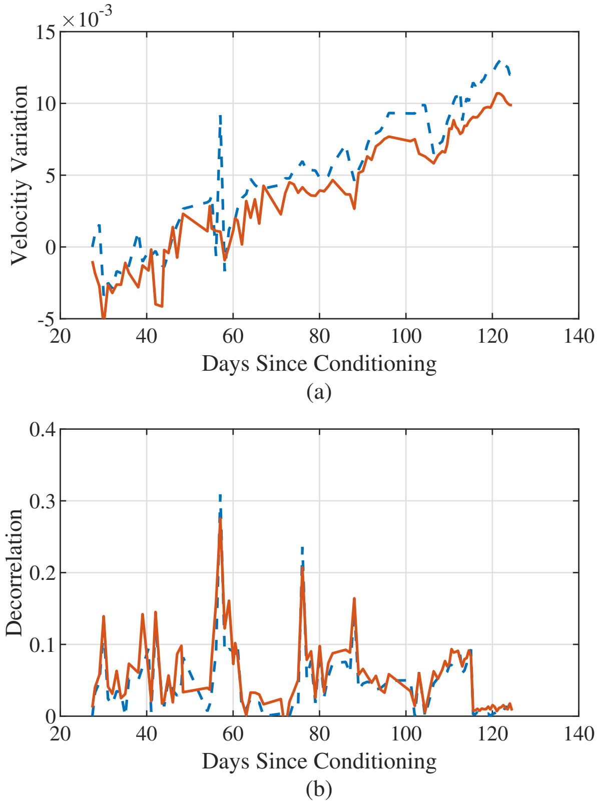

Fig. 14. Comparison of (a) velocity variation and (b) decorrelation between reconstructed values and calculated values using S1 data collected from unconfined control specimen using a standard autoencoder.

measurements, which had the largest increase during the experiment.

D. Data Set Composition

The experiment for this paper was conducted using seven different data sets, one training data set and six testing data sets. The training data consists of all of the data collected for the two control specimens, the unconfined control specimen and the confined control specimen. For the unconfined control specimen, S1 collected 709 samples, while S2 and S3 only collected 116 samples as they were removed during the experiment. For the confined control specimen, which only had one sensor S1, 593 samples were collected. After rearranging the data from each of the sensors into sequences of length sixteen and then combining them, the total number of sequences used for training was 1474.

For the testing data sets, data from each sensor of each reactive specimen comprised its own testing data set, resulting in a total of six testing data sets. Furthermore, because we are focused on when the initial damage occurs in concrete specimens undergoing ASR damage, only the data from the first four months of the experiment was used. Each sensor of the reactive specimens collected 116 samples, resulting in 101 sequences used for each testing data set.

IV. Results and Discussion

As described in section II-B, the reconstruction-error based anomaly detection model is developed using the data from the two control specimens. Using the model described in section II-C.3 the model was able to achieve a low training loss of 0.000198. To visualize how well the model reconstructs the velocity variation and decorrelation values of the training data, the reconstructed values are compared with the calculated values from the measurements in Fig. 8 using sensor S1 from the unconfined control specimen as an example.

The reconstruction error of the model using the training data, shown in Fig. 9, is used to choose the reconstruction error threshold for the model. Using the IQR, as described in section II-B, the threshold is chosen to be 0.000470. The reconstruction error threshold will be then used to determine which input data sequence is anomalous. Sequences which returned a reconstruction error greater than the threshold will be classified as anomalous while sequences which returned reconstruction errors less than the threshold will be classified as normal.

The trained anomaly detection model is then applied to data collected from different sensors on the reactive specimens to test the model's ability to detect early damage in concrete structures undergoing ASR. The reconstruction errors of the model for each sensor from each reactive specimen and its corresponding first anomaly detection date are shown in Fig. 10. As demonstrated in Figure 10, for each sensor, the reconstruction errors of most data points are below the threshold before the first anomaly detection date, which can be more clearly observed in Fig. 11, a zoomed-in plot before the first anomaly date of S2 from the unconfined reactive specimen. On average, only twenty-one sequences had reconstruction errors above the threshold before the first anomaly detection date, and the average reconstruction error before the first anomaly detection date was 0.0043. The average reconstruction error before the first anomaly detection date is boosted by a few points which had large reconstruction errors. These samples with unusually large errors occurred right after chamber shutdowns, which were necessary for expansion measurements and sensor reinstallations. The effect of the chamber shutdown may have contributed to these large errors before the first anomaly detection date. Furthermore, although the reconstruction errors of some data points before the first anomaly date are above the threshold, they are not, however, classified as anomaly dates because they do not satisfy the criterion of having sixteen or more consecutive data points over the threshold, as stated in section II-B. After the first anomaly detection date, in general, the reconstruction error of each sensor does not fall below the threshold, and tends to increase with time. The average reconstruction error after the first anomaly detection date is 0.1791, which is significantly larger than the average reconstruction error before the first anomaly detection. The first date that anomalies were detected by all sensors are also summarized in Table II. From Table II we can see that the first anomaly detection dates of all sensors except S3 from the unconfined specimen are within the date range (between days 69 and 84) during which the average expansion begins to increase significantly as demonstrated in Fig. 7. These results demonstrate the feasibility of using the developed LSTM-CNN autoencoder model and the coda wave signals to detect early damage in concrete structures.

In addition, Table II shows that the date at which each sensor detects the first anomaly may vary. The variation of anomaly dates detected by different sensors may be explained by the sensitivity kernels of coda-wave interferometry that show high sensitivity around the direct path between source and receiver [30]. Use S1 and S3 as examples. Since the transmitter was placed opposite to S1 and S1 is closer to side C of each specimen, the anomaly date detected by S1 might be more correlated to the transverse expansion measured on side C, compared with that detected by S3. Similarly, the anomaly date detected by S3, which is closer to side D of each specimen, might be more correlated to the transverse expansion measured on side D. This phenomenon is observed in both unconfined and confined reactive specimens.

As shown in Fig. 12(a), for the unconfined specimen, the transverse expansion measured on side C shows a significant increase between measurements taken on day 69 and day 84, while that on side D does not start to increase significantly until between days 84 and 97. Accordingly, S1 detects anomaly on day 79, earlier than S3 that detects anomaly on day 92. For the confined specimen, as shown in Fig. 12(b), the transverse expansion measurements on both sides C and D start to increase significantly between days 69 and 84. As a result, both S1 and S3 detect anomaly on the same day.

As a baseline comparison anomaly detection using the same coda-wave features was conducted using an one-class support vector machine (SVM). For the one-class SVM a radial basis function (RBF) kernel was used for non-linear mapping and the parameter ν, which determines the upper bound on the fraction of outliers and the lower bound on the number of support vectors [31], and the parameter γ of the RBF kernel which determines how far the influence of a single training example reaches, were tuned so that the radius of the decision boundary containing most of the data was minimized [32]. A ν value of 0.05 and a γ value of 10 best minimized the radius of the decision boundary while containing most of the data as shown in Fig. 13.

The distribution of the control data, as well as the decision boundary determined by the one-class SVM can be seen in Fig. 13(a). From the figure it can be seen that there are three main clusters of data for the training data set. The boundary decision encompasses most of the middle cluster and extends towards the cluster to the right which has a higher density than the cluster to the left.

The distribution of the testing data for S2 of the unconfined reactive specimen and the decision boundary can be seen in Fig. 13(b). A few of the points lie within the decision boundary, but majority of the data exists outside of the decision boundary as the velocity variation decreases far more for the unconfined reactive specimen. Fig. 13(b) showed the results obtained using the testing data for S2 of the unconfined reactive specimen, because it deviated most significantly from our expectations, but the results using all of the sensors are summarized in Table III.

The one-class SVM detected anomaly dates that were generally earlier than that of the proposed method. In particular, S2 of both the unconfined and confined reactive specimens detected an anomaly much earlier than the expected damage date, day 62 and 60 respectively. Based on the expansion of the reactive specimens in Fig. 7, there is little evidence to suggest damage is occurring before day 69, suggesting that the one-class SVM is detecting anomalies before damage occurs.

Another method used as comparison to the proposed method was a reconstruction-error-based anomaly detection method using an autoencoder with no recurrent or convolutional layers. The same training and testing steps were taken for this method, and the anomaly detection dates using this method but a training loss of only 0.000713 was achieved, more than three times greater than the training loss achieved by the proposed method. First anomaly detection dates have been summarized in Table IV. To visualize how well this model reconstructs the velocity variation and decorrelation values of the training data, the reconstructed values are compared with the calculated values from the measurements in Fig. 14 using sensor S1 from the unconfined control specimen as an example. As seen in Fig. 14, the standard autoencoder which does not include recurrent or convolutional layers was unable to reconstruct the input sequences as accurately as the proposed method, as seen in Fig. 8. The first anomaly detection dates for the standard autoencoder method as shown in Table IV is very similar to that of the one-class SVM method. As stated before, it is unlikely that a change occurred in the material before day 69, suggesting that the two comparison methods are detecting anomalies before damage has occurred.

V. Conclusion

An anomaly detection model based on coda waves is investigated for early damage detection of concrete structures undergoing ASR, and its feasibility is demonstrated. The model trained on data from multiple undamaged concrete structures is used to detect early damage in two different ASR specimens. By making use of the advantages of convolutional and recurrent layers, an autoencoder was trained to achieve a very low training loss of 0.000198. A reconstruction error threshold was chosen using interquartile ranges of the reconstruction errors of the training data. When the reconstruction error of the ASR specimens exceeds the threshold, the input sequence is marked as an anomaly. An anomaly date for each specimen is detected when all sequences containing data from that date is marked as anomalous. The experimental validation results show that the anomaly dates detected by the developed model are consistent with that derived from the expansion measurements, which demonstrates that the model developed from control specimens can be used for detecting initiation of damages in different specimens. Previous works have used damage detection and damage prediction methods which were dependent on specimen specific metrics. However, the proposed method has been shown to be able to detect damage in concrete undergoing ASR for two different specimens. The proposed method is trained on data from completely different specimens and has shown to be able to make predictions for two different test specimens, suggesting that it can be generalized across specimens. With more undamaged concrete specimens, the proposed method will likely be able to better reconstruct data of normal data, improving the performance and robustness of the proposed method. In addition, the anomaly dates detected by sensors at different locations seem to be highly correlated to the expansion measurements at locations and directions close to the direct path between source and receiver, consistent with the conclusions derived by other researchers based on the sensitivity kernels of coda-wave interferometry.

VI. Acknowledgement

This research is supported in part by the U.S. Department of Energy - Nuclear Energy University Program (NEUP) under the contract DE-NE0008544.

References

[1] T. E. Stanton, "Expansion of concrete through reaction between cement and aggregate," *Transactions of the American Society of Civil Engineers*, vol. 107, no. 1, pp 54–84, Jan. 1942, DOI: 10.1061/taceat.0005540.

[2] M. G. Peterson, "A chemoplastic model for alkali-silica expansion: effect of stress-induced anisotropy," M.S. thesis, Dept. of civil and environmental engineering, Massachusetts Institute of Technology, Boston, MA, 2000.

[3] K. Aki and B. Chouet, "Origin of coda waves: source, attenuation, and scattering effects," *Journal of Geophysical Research*, vol. 80, no. 23, pp. 3322–3342, 1975, DOI: 10.1029/JB080i023p03322.

[4] T. Planés and E. Larose, "A review of ultrasonic coda wave interferometry in concrete," *Cement and Concrete Research*, vol. 53, pp. 248–255, Nov. 2013, DOI: 10.1016/j.cemconres.2013.07.009.

[5] C. L. Nogueira and K. L. Rens, "Effect of acoustoelasticity on ultrasonic pulses and damage of concrete under tensile stress," *ACI Materials Journal*, vol. 115, no. 3, pp. 381–391, May. 2018, DOI: 10.14359/51702184.

[6] D. P. Schurr, "Monitoring damage in concrete using diffuse ultrasonic coda wave interferometry," M.S. thesis, Dept. of civil engineering, Georgia Institute of Technology, Atlanta, GA, 2010.

[7] Y. Zhang, O. Abraham, F. Grondin, A. Loukili, V. Tournat, A. L. Duff, B. Lascoup, and O. Durand, "Study of stress-induced velocity variation in concrete under direct tensile force and monitoring of the damage level by using thermally-compensated coda wave interferometry," *Ultrasonics*, vol. 52, no. 8, pp. 1038–1045, Dec. 2012, DOI: 10.1016/j.ultras.2012.08.011.

[8] E, Niederleithinger, X. Wang, M. Herbrand, and M. Müller, "Processing ultrasonic data by coda wave interferometry to monitor load tests of concrete beams," *Sensors*, vol. 18, no. 6, Jun. 2018, DOI: 10.3390/s18061971.

[9] E. Larose, T. Planes, V. Rossetto, and L. Margerin, "Locating a small change in a multiple scattering environment," *Applied Physics Letters*, vol. 96, no. 20,, May. 2010, DOI: 10.1063/1.3431269.

[10] R. Thery, A. Guillemot, O. Abraham, and E. Larose, "Tracking fluids in multiple scattering and highly porous materials: toward applications in non-destructive testing and seismic monitoring," *Ultrasonics*, vol. 102, Mar. 2020, DOI: 10.1016/j.ultras.2019.106019.

[11] Y. Zhang, T. Planés, E. Larose, A. Obermann, C. Rospars, and G. Moreau, "Diffuse ultrasound monitoring of stress and damage development on a 15-ton concrete beam," *The Journal of the Acoustical Society of America*, vol. 139, no. 4, pp. 1691–1701, Apr. 2016, DOI: 10.1121/1.4945097.

[12] E. Larose and S. Hall, "Monitoring stress related velocity variation in concrete with a 2×10-5 relative resolution using diffuse ultrasound," *The Journal of the Acoustical Society of America*, vol. 125, no. 4, pp. 1853–1856, Apr. 2009, DOI: 10.1121/1.3079771.

[13] T. Planés, E. Larose, V. Rossetto, and L. Margerin, "Imaging multiple local changes in heterogeneous media with diffuse waves," *The Journal of the Acoustical Society of America*, vol. 137, no. 2, pp. 660–667, Feb. 2015, DOI:10.1121/1.4906824.

[14] V. Chandola, A. Banerjee, and V. Kumar, "Anomaly detection: a survey," *ACM Computing Surveys*, vol. 41, no. 3, Jul. 2009, DOI:10.1145/1541880.1541882.

[15] G. Jiang, P. Xie, H. He and J. Yan, "Wind turbine fault detection using a denoising autoencoder with temporal information," *IEEE/ASME Transactions on Mechatronics*, vol. 23, no. 1, pp. 89-100, Feb. 2018, DOI: 10.1109/TMECH.2017.2759301.

[16] V. Alex, K. Vaidhya, S. Thirunavukkarasu, C. Kesavadas, and G. Krishnamurthi, "Semisupervised learning using denoising autoencoders for brain lesion detection and segmentation," *J. Med. Imag*, vol. 4, no. 4, Dec. 2017, DOI: 10.1117/1.JMI.4.4.041311.

[17] J.K. Chow, Z. Su, J. Wu, P. S. Tan, X. Mao, and Y. H. Wang, "Anomaly detection of defects on concrete structures with the convolutional autoencoder," *Advanced Engineering Informatics*, vol. 45, Aug. 2020, DOI: 10.1016/j.aei.2020.101105.

[18] R. Snieder, "Coda wave interferometry for estimating nonlinear behavior in seismic velocity," *Science*, vol. 295, no. 5563, pp. 2253-2255, Mar. 2002. DOI: 10.1126/science.1070015.

[19] P.J. Rousseeuw and M. Hubert, "Anomaly detection by robust statistics," *WIREs Data Mining and Knowledge Discovery*, vol. 8, no. 2, Mar. 2018, DOI: 10.1002/widm.1236.

[20] O. I. Lobkis and R. L. Weaver, "Coda-Wave Interferometry in Finite Solids: Recovery of P -to- S Conversion Rates in an Elastodynamic Billiard," *Phys. Rev. Lett.*, vol. 90, no. 25, Jun. 2003, DOI: 10.1103/PhysRevLett.90.254302.

[21] C. Hadziioannou, É. Larose, O. Coutant, P. Roux, and M. Campillo, "Stability of monitoring weak changes in multiply scattering media with ambient noise correlation: laboratory experiments," *The Journal of the Acoustical Society of America*, vol. 125, no. 6, pp. 3688–3695, Apr. 2009, DOI: 10.1121/1.3125345.

[22] R. Zotz-Wilson, T. Boerrigter, and A. Barnhoorn, "Coda-wave monitoring of continuously evolving material properties and the precursory detection of yielding," *The Journal of the Acoustical Society of America*, vol. 145, no. 2, pp. 1060–1068, Feb. 2019, DOI:10.1121/1.5091012.

[23] K. Singh and S. Upadhyaya, "Outlier detection: applications and techniques," in *International Journal of Computer Science Issues*, vol. 9, issue 1, no. 3, 307 – 323, Jan. 2012, DOI: 10.1.1.402.6378.

[24] A. C. Müller and S. Guido, "Model evaluation and improvement," in *Introduction to Machine Learning with Python: A Guide for Data Scientists*, 1st ed., Sebastopol, CA, USA: O'Reilly Media, Inc, 2016, ch. 6, sec. 9, pp. 249–251.

[25] J. Zhao, X. Mao, and L. Chen, "Speech emotion recognition using deep 1D & 2D CNN LSTM networks," *Biomedical Signal Processing and Control*, vol. 47, Jan. 2019, DOI: 10.1016/j.bspc.2018.08.035.

[26] Z. He, J. Zhou, H. Dai and H. Wang, "Gold Price Forecast Based on LSTM-CNN Model," in *2019 IEEE Intl Conf on Dependable, Autonomic and Secure Computing, Intl Conf on Pervasive Intelligence and Computing, Intl Conf on Cloud and Big Data Computing, Intl Conf on Cyber Science and Technology Congress (DASC/PiCom/CBDCom/CyberSciTech)*, Fukuoka, Japan, 2019, pp. 1046-1053, DOI: 10.1109/DASC/PiCom/CBDCom/CyberSciTech.2019.00188.

[27] C. Malone, "Quantitative assessment of alkali-silica reaction in small and large concrete specimens utilizing nonlinear techniques," M.S. thesis, Dept. of civil engineering, Univ. of Nebraska-Lincoln, Omaha, NE, 2020.

[28] H. Sun, Y. Tang, C, Malone, J. Hu, and J. Zhu, "Ultrasonic-Acoustic Emission Hybrid System for Monitoring Concrete Structures Affected by Alkali-silica Reaction," in *The 12th International Workshop on Structural Health Monitoring (IWSHM19)*, Stanford, CA, USA, 2019, DOI: 10.12783/shm2019/32406.

[29] H. Sun, "Thermal modulation of nonlinear ultrasonic waves," Ph.D. dissertation, Dept. of civil engineering, Univ. of Nebraska-Lincoln, Omaha, NE, 2020.

[30] L. Margerin, T. Planés, J. Mayor, and M. Calvet, "Sensitivity kernels for coda-wave interferometry and scattering tomography: theory and numerical evaluation in two-dimensional anisotropically scattering media," *Geophys. J. Int.*, vol. 204, no. 1, Jan. 2016, DOI: 10.1093/gji/ggv470.

[31] B. Schölkopf, R.C. Williamson, A.J. Smola, J. Shawe-Taylor, and J.C. Platt, "Support vector method for novelty detection," in *Proceedings of the 12th International Conference on Neural Information Processing Systems*, Denver, CO, USA, 1999, pp. 582–588, DOI: 10.5555/3009657.3009740.

[32] Y. Guerbai, Y. Chibani, and B. Hadjadji, "The effective use of the one-class SVM classifer for handwritten signature verification based on writer-independent parameters," in *Pattern Recognition*, vol. 48, no. 1, pp 103 – 113, Jan. 2015, DOI: 10.1016/j.patcog.2014.07.016.